Two-dimensional optical spectroscopy by periodic excitation of sublevel coherence with sub-Doppler resolution

G. Wäckerle, St. Appelt, and M. Mehring
2. Physikalisches Institut, Universität Stuttgart, Pfaffenwaldring 57, D-7000 Stuttgart 80, Federal Republic of Germany
(Received 26 July 1990)

The response of ground-state spin coherence to narrow-band periodic optical excitation is studied theoretically and experimentally. The dependence of the induced oscillating magnetization on the transverse magnetic field and on the frequency of the laser radiation is calculated for a four-level model system from a Bloch-type equation, yielding a two-dimensional resonance line. The application of this two-dimensional high-resolution Zeeman and optical spectroscopy is demonstrated experimentally in the case of the D_1 line of atomic rubidium vapor. Resolution in the kilohertz range is achieved, which allows clear spectral separation of the two isotopes ^{85}Rb and ^{87}Rb, showing overlapping lines in the conventional optical absorption spectrum.

I. INTRODUCTION

In optical pumping spectroscopy[1] it is well known that the transmitted light intensity is modulated by irradiating the system with resonant radio-frequency (rf) fields.[2–5] By monitoring the transmission of light as a function of the rf, sublevel splittings of the optically connected states can thus be measured, which are usually not resolved in the Doppler-broadened optical spectrum.

Shortly after this rf-optical double-resonance technique was established theoretically[2,3] and experimentally[4,5] it has been shown that the same information on sublevel splittings can be obtained by purely optical means, if the pumping light intensity is amplitude modulated at a frequency close to the Larmor frequency and a precessing spin polarization is observed. This idea of Bell and Bloom has recently experienced a revival in high-resolution spectroscopy, where pulse trains of mode-locked picosecond dye lasers were used as "modulated" light sources.[6,7]

When a light pulse short compared to the Larmor period traverses the sample, a small amount of magnetic polarization along the propagation direction of the light is created in the ground state. This polarization "packet" starts to precess around the external constant magnetic field, which is perpendicular to the pump direction. If the pulse repetition rate (or its higher harmonics) of the laser matches the precession frequency of the consecutively pumped polarization packets, these packets are reinforced by the subsequent pumping events and add up constructively to yield a macroscopic precessing magnetization, where the precession frequency corresponds to the nearly degenerate ground-state splitting. This macroscopic magnetization introduces an anisotropic time-dependent optical susceptibility in the sample, which is readily observable by polarization-sensitive optical probe techniques. By such an experimental procedure it is possible to measure ground-state Zeeman and hyperfine splittings and linewidths in gases[7,8] and solids[9] with ultimate resolution. More recently, a similar excitation scheme utilizing the matching of excitation pulse repetition rates with "internal" frequencies of the system under investigation has been employed in the field of impulsive stimulated Raman scattering (ISRS) in crystalline solids.[10]

In frequency space the experiment can be described as follows. The amplitude modulation introduces sidebands to the optical carrier frequency at a separation given by the modulation frequency, i.e., the pulse repetition rate. If the sideband separation equals the sublevel splitting, coherences in the ground state can be pumped in a stimulated Raman-type process.

In this contribution we do not focus on the high-resolution aspect of this kind of spectroscopy but rather on the selectivity of the preparation and detection scheme with respect to different ground-state splittings of the atoms under investigation, which has not been applied in the optical regime so far. However, the selective excitation of sublevel coherence by periodic irradiation closely resembles the delays alternating with nutation for tailored excitation (DANTE) pulse sequence, well known in selective spin excitation in NMR.[11]

Suppose there are isotopes in the atomic vapor, which differ in their ground-state splittings and have overlapping optical spectra. We show that the method described here is capable of separating the optical spectra of all the isotopes in the sample by means of the highly selective excitation of sublevel coherence by modulated pumping light. To be specific, assume that the isotopic species only differ by their ground-state gyromagnetic ratios. In a constant magnetic field the Zeeman resonance can be obtained by choosing the proper pulse repetition rate of the pumping light for one isotope only. Due to the different gyromagnetic ratios of the pumped magnetization packets for all other species interfere destructively and do not lead to a macroscopic polarization, which could be detected by the weak probe beam. Besides the sublevel resonance condition also the optical field has to be close to resonance in order to pump the polarization packets. Setting the sublevel resonance condition for one

isotope and scanning the optical wavelength yields the optical spectrum of only the "tagged" species, whereas all others are suppressed. In this way, complicated overlapping optical spectra may be unraveled with sub-Doppler resolution. The feasibility of this new method is demonstrated with rubidium vapor in natural abundance, where two isotopes, ^{85}Rb (72 at.%) and ^{87}Rb (28 at.%) are present.

Our work is an extension of ground-state spectroscopy by excitation of sublevel coherence into the optical domain, which is most clearly demonstrated in the two-dimensional (2D) spectra obtained with our method. We used periodic optical pumping of ground-state spin coherence to separate optical spectra belonging to different ground states, which has not been reported before.

The paper is organized as follows. In Sec. II we present the simple theoretical model to describe our experiments and the principle of the experiment is introduced. The experimental setup is given in Sec. III together with a comprehensive description of the real atomic system experimentally investigated, which is by far more complicated than the four-level system introduced in Sec. II. In Sec. IV experimental results for the atomic rubidium sample are shown and discussed.

II. THEORETICAL TREATMENT

To introduce the basic ideas of the experiment, we start with the four-level model system depicted in Fig. 1(a). Levels 1 and 2 correspond to the nearly degenerate $J=\frac{1}{2}$ ground-state split by the Zeeman interaction of its magnetic dipole moment with the external field B. We adopt the quantization axes convention of Ref. 12 [see Fig. 1(b)] and similar notation. Pump pulses and probe beam travel within a small angle along the z axis, which is the quantization axis, the magnetic field is directed along x, and y completes the orthogonal axes system. The sublevel splitting of the $J'=\frac{1}{2}$ excited state may differ from the ground-state splitting due to different magnetic moments of the two electronic states.

With right (left) circularly polarized pumping light only transition $1\rightarrow 4$ ($2\rightarrow 3$) is induced, in connection with the spontaneous decay of the upper levels creating a population difference within the ground state. This non-Boltzmann population corresponds to an atomic spin polarization which decays at a rate Γ. In the case where excited-state population and optical coherences are negligible, it has been shown that the dynamics of the ground-state spin sublevels can be cast into the Bloch-type equation[12,13]

$$\dot{\mathbf{m}}=\mathbf{\Omega}\times\mathbf{m}-\Gamma_{\text{eff}}\mathbf{m}+\mathbf{P}\ , \tag{2.1}$$

with $\mathbf{\Omega}=(\Omega_x,\Omega_y,\Omega_z)=(\Omega_L,0,P_+\bar{\Delta})$, $\mathbf{P}=(0,0,P_+)$, and $\Gamma_{\text{eff}}=\Gamma+P_+$. The components of the magnetic polarization vector $\mathbf{m}$ are constructed from the density matrix of the ground-state two-level system (1,2) according to the Feynman-Vernon-Hellwarth theorem.[14] $\Omega_L=\gamma_J B$ is the Larmor frequency, where $\gamma_J=2\pi\mu_B g_J/h$ is the effective gyromagnetic ratio of the ground state, μ_B is Bohr's magneton, and g_J is the Landé factor. $\bar{\Delta}=\Delta/\Gamma_2$ is the optical resonance offset normalized to the homogeneous optical linewidth Γ_2. $P_+=P_0/(1+\bar{\Delta}^2)$ is the rate right circularly polarized light creates polarization, where $P_0=\beta^2/\Gamma_2$ and β is the optical Rabi frequency. The optical pumping rate P_+ traces the homogeneous line profile and is largest at the optical line center ($\bar{\Delta}=0$). The effective relaxation rate Γ_{eff} contains P_+ to model the destruction of coherence by the optical pumping process, and a light-independent term Γ, which is given by the rate the atoms escape from the laser beam region and/or relax by spin-lattice relaxation processes. It is noted that the pumping light introduces an inhomogeneity $\mathbf{P}$ to the Bloch-type equation (2.1), which turns into the well-known homogeneous Bloch equation under light-off conditions ($P_+=0$).

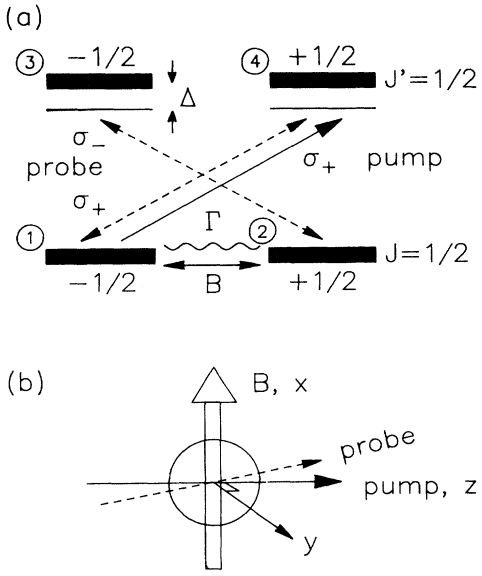

FIG. 1. (a) Energy-level scheme of the four-level ($J=\frac{1}{2},J'=\frac{1}{2}$) model system after Ref. 12. The quantization axis is chosen parallel to the propagation direction of the laser beam. The pump beam of σ_+ polarization (solid arrow) induces transition $1\rightarrow 4$ and the linearly polarized probe beam is decomposed into σ_+ and σ_- light (dashed arrows). Transitions between substates are induced by the B field and coherences relax with a rate Γ (wavy line). The optical frequency is off resonant by Δ. (b) Schematic of beam and field directions used in the experiment. The circle in the center represents the vapor cell. Within a very small angle pump (solid line) and probe beam (dashed line) both point along the z direction, which is the quantization axis. The constant magnetic field B is transversal and points along the x axis and y completes the orthogonal axes system.

We solved Eq. (2.1) for the periodic optical excitation scheme depicted in Fig. 2(a). The pump light is on for times $t_1\le t<t_2$ and is off for $t_2\le t<t_3$, where the periodicity of this simple excitation sequence is $t_3-t_1=T$. In the first interval (I) of duration $t_2-t_1=t_p$ the inhomogeneous equation has to be solved, yielding $\mathbf{m}(t_2)$, which still contains arbitrary constants of integration for the three vector components. In this interval (I) the magnetization oscillates with an effective frequency $\Omega=(\Omega_L^2+P_+^2\bar{\Delta}^2)^{1/2}$ and is damped exponentially with

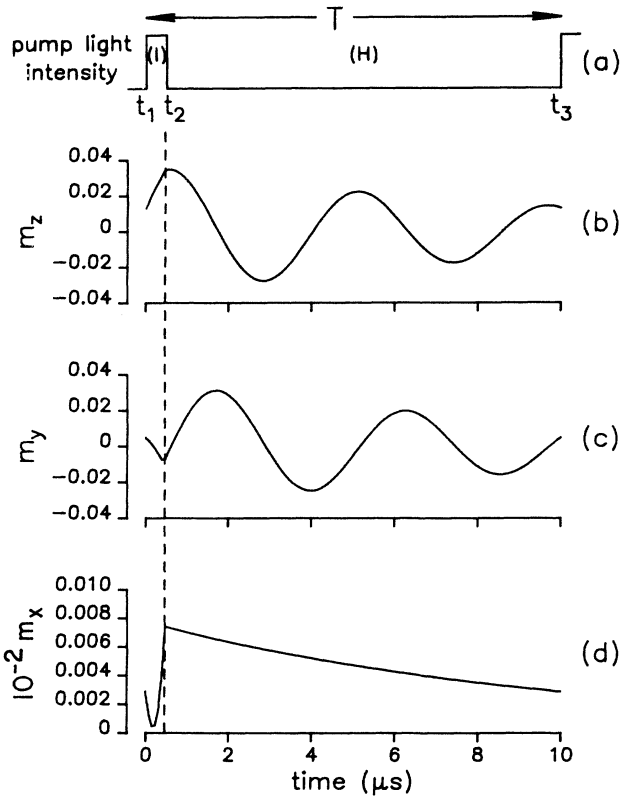

FIG. 2. (a) Periodic excitation sequence for which the Bloch-type equation (2.1) is solved. The pump pulse is on during interval (I) for a time $t_p=t_2-t_1$ and is off during interval (H). The period of the excitation sequence is $T=t_3-t_1$ and is chosen to be twice the Larmor period for this calculation. (b)–(d) calculated time dependence of the magnetization vector $\mathbf{m}$. The z component (b) is detected in the experiments. Note that the y component m_y (c) is in quadrature phase with respect to m_z. The x component m_x (d) only appears if the effective field Ω has a z component, i.e., $\bar{\Delta}\neq 0$. In the interval (H) m_x relaxes monotonically because it is parallel to the static B field. The vertical dashed line marks the end of the pump pulse, from where the magnetization precesses freely around the x axis and decays at a rate Γ. The displayed curves are calculated with $P_0=10^6\ \mathrm{s}^{-1}$, $\Gamma=10^6\ \mathrm{s}^{-1}$, $\bar{\Delta}=1$, $t_p=4.7\times10^{-6}$ s, $T=10^{-5}$ s, $\Omega_L/2\pi=2.2\times10^5\ \mathrm{s}^{-1}$, and $k=2$.

the effective rate $\Gamma_{\mathrm{eff}}=\Gamma+P_+$. In the second interval (H) the homogeneous Eq. (2.1) with $\mathbf{P}=\mathbf{0}$ has to be solved with $\mathbf{m}(t_2)$ calculated from (I) as the initial condition. In this interval (H) we have a free precession of the magnetization with the frequency Ω_L and relaxation rate Γ. The stationary solution for the entire period $t_1\leq t<t_3$ is found by searching for solutions, which have the periodicity of the excitation cycle, i.e.,

$$\mathbf{m}(t)=\mathbf{m}(t+nT)\ , \tag{2.2}$$

where n is an integer. This condition determines the integration constants unambiguously and the solution for the given excitation sequence is obtained.

We get a quasistationary magnetization in a sense that it clearly is time dependent within the excitation period but is invariant under translations of nT in time forced by the condition of Eq. (2.2). This fact is in close analogy to the Bloch wave functions of electrons in solid-state physics, which are invariant under lattice translations in space and are obtained by introducing periodic boundary conditions to the Schrödinger equation containing a potential with lattice periodicity.

Figures 2(b)–2(d) show the three components of the magnetization vector $\mathbf{m}$ for one period, calculated from Eq. (2.1) satisfying Eq. (2.2), where the Larmor period is chosen so that $2T_L\approx T$. As seen from Figs. 2(b)–2(d) we get $\mathbf{m}(t_1)=\mathbf{m}(t_3)$ for the magnetization, which is implied by Eq. (2.2). In general, at a fixed instant of time relative extrema of the components $m_i(t)$, $(i=x,y,z)$ are obtained when

$$kT_L\approx T=1/\nu_{\mathrm{rep}}\quad (k=1,2,3,\ldots) \tag{2.3}$$

leading to the kth-order Zeeman resonance. In addition to these Zeeman resonances also optical resonance is found when detuning from optical resonance is small ($\bar{\Delta}\approx 0$) except for the x component, which vanishes in this case. The latter is a consequence of the effective field Ω not pointing in the $\mathbf{B}$ direction, if an off-resonance light pulse is present.

In order to introduce a considerable amount of optically pumped ground-state magnetization by periodic excitation, both optical and Zeeman resonance conditions have to be met. The optical resonance can be adjusted by tuning the laser close to the absorption wavelength of the sample and the latter can be adjusted either by setting the repetition rate ν_{rep} of the pump pulse at a fixed field B or by scanning the B field keeping the repetition rate fixed, according to Eq. (2.3). This two-dimensional resonance behavior is shown in Fig. 3, where a contour plot of the length of the yz projection of the magnetization vector, $m_{yz}(t_2)=[m_y^2(t_2)+m_z^2(t_2)]^{1/2}$, is depicted as a function of the Larmor frequency Ω_L and the optical detuning Δ for a fixed pump pulse repetition rate ν_{rep}. Both axes are normalized to their corresponding homogeneous relaxation rates Γ and Γ_2, respectively. The Larmor frequency range is set to include second-order Zeeman resonance ($k=2$) only. The Zeeman resonance line for the optical on-resonance case can be considered as the horizontal cross section through the resonance peak of the two-dimensional resonance landscape $m_{yz}(\bar{\Delta},\Omega_L)$, whereas the vertical cross section would show the optical resonance line of the atom for which the Zeeman resonance is set according to Eq. (2.3). The linewidths in the two dimensions are on the order of the assumed homogeneous relaxation rates Γ_2 and Γ for the optical and Zeeman transition, respectively. The starlike pattern reflects the Lorentzian line shapes and is well known in 2D NMR.[15]

The analytic expressions obtained from solving Eq. (2.1) under the condition of Eq. (2.2) do not give much insight into the two-dimensional resonance behavior due to their complicated lengthy structure. They are not reproduced here. Because we measure the precessing magnetization by lock-in techniques, rather a Fourier analysis of response to the periodic excitation is applied, which is summarized in the Appendix. If one is interested in the

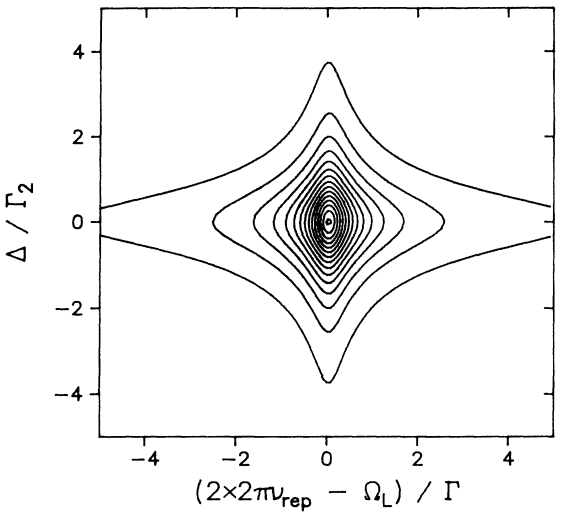

FIG. 3. Calculated two-dimensional plot of $m_{yz}(t_2)$, the length of the magnetization vector at the end of the pump pulse projected into the yz plane. The vertical axis is the optical detuning Δ from exact resonance of the four-level model system normalized to the homogeneous optical linewidth Γ_2. The horizontal axis is the deviation of the Larmor frequency Ω_L from twice the repetition rate of the light pulses (second-order Zeeman resonance) normalized to the homogeneous linewidth Γ of the ground-state Zeeman sublevels. The contour plot lines connect points of equal values of $m_{yz}(t_2)$. Here, $P_0=10^4$ s^{-1}, $\Gamma=3\times10^4$ s^{-1}, $t_p=10^{-7}$ s, $T=10^{-5}$ s.

full time evolution of the magnetization within the period, the above-mentioned analytic solution has to be consulted, however.

The components of $\mathbf{m}(t)$ can be detected by a weak linearly polarized probe beam. The optical susceptibilities for left and right circularly polarized light (into which the probe can be decomposed) are determined by the magnetization component along the propagation direction of the probe beam, in our case the z axes. Since $m_z(t)$ is time dependent, also the absorption coefficients and indices of refraction for σ_+ and σ_- light vary with time according to[12]

$$\alpha_\pm=\alpha_0[1\pm m_z(t)], \tag{2.4}$$

$$n_\pm=1+(n_0-1)[1\pm m_z(t)]\ , \tag{2.5}$$

where the α_0 and n_0 are the absorption coefficient and the index of refraction of the unpolarized medium, respectively. The presence of magnetization m_z can thus be measured with the polarimeter setup discussed in Sec. III. Depending on the operational mode of the polarimeter either the difference in absorption $(\alpha_+-\alpha_-)$ is measured, which corresponds to the magnetic circular dichroism (MCD), or the difference n_+-n_- is recorded, which leads to magneto-optical rotation (MOR) of the polarization direction of the probe beam. As a function of the optical wavelength the two quantities are Kramers-Kronig related and show absorptive $[\propto 1/(1+\bar{\Delta}^2)]$ and dispersive $[\propto \bar{\Delta}/(1+\bar{\Delta}^2)]$ line shapes for MCD or MOR, respectively. The detected signal will thus be the product of the created magnetization (Fig. 3) and the MCD or MOR detection sensitivities.

III. EXPERIMENT

The experiments were performed on the $5\,^2S_{1/2}$ ground state of natural abundance atomic rubidium with a nitrogen buffer gas pressure of $p(N_2)=30$ mbar. The sample was placed in a 3-cm glass sphere coated with $Si(CH_3)_3Cl$ from the inside. The Rb number density was controlled by actively stabilizing the temperature of a hot air stream that heated the sample to 70 °C for the experiments described here. This corresponds to $n_{Rb}=6.8\times10^{11}$ cm^{-3}. The experimental arrangement is schematically shown in Fig. 4. As an optical source we used a single-mode $Al_xGa_{1-x}As$ diode lasser (Hitachi, HL7801) with approximately 3-mW output power in the spectral region of interest. The laser head and electronics were thermally stabilized as described earlier.[16] The frequency jitter was less than 200 MHz on the time scale of the experiment. Wavelength tuning was performed by slowly scanning the injection current.

For optical pumping the D_1 lines of the two isotopes were used throughout, falling in a narrow range around 795 nm. The laser was split into a circularly polarized pump beam (90%) and a weaker linearly polarized probe beam (10%), both traversing the sample perpendicular to the magnetic field B. The angle between pump and probe beam was less than 1°, both beams having a diameter of approximately 0.5 mm at the sample cell. The magnetic

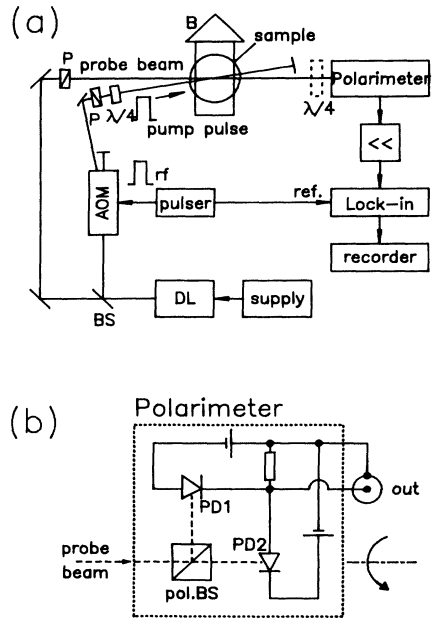

FIG. 4. (a) Experimental setup. DL, thermally stabilized diode laser; BS, beam splitter; P, polarizer; λ/4, quarter wave retardation plate; AOM, acousto-optic modulator. (b) Construction of the polarimeter detector. pol BS, polarizing beam splitter; PD_1, PD_2, photodiodes. The polarimeter is as a whole rotatable around the incident probe beam direction.

field B is produced by a split solenoid and the earth's field is compensated for by a set of orthogonal Helmholtz coils. The pump beam is gated by a transistor-transistor-logic (TTL) -driven acousto-optic modulator (A&A, MT-08) and is blocked after the sample. The probe beam is constantly on and is fed to the polarimeter detector after having traversed the gas cell.

The polarimeter[17,18] is built from a polarizing beam splitter and two photodiodes (EG&G, FND100Q) that are connected subtractively. The entire device can be rotated around the probe beam axis to adjust zero output, when the two photocurrents are equal. The nulling procedure is done at a blocked pump beam. Due to the nulled bridgelike arrangement we have very high sensitivity with respect to rotations of the polarization direction (MOR) of the linearly polarized probe beam. Faraday rotation angles as small as 50 μrad are readily detectable. To measure the MCD instead of the MOR, a $\lambda/4$ retardation plate is placed in front of the polarimeter. The polarimeter output is fed to a video amplifier and subsequently is phase sensitively detected by a lock-in amplifier at a reference frequency $k\nu_{\rm rep}$ that is an integer multiple of the pulse repetition rate. Thus the kth-order Zeeman resonance is detected.

The pulsed optical pumping cycle is kept constant at duty cycles of less than 1/10 at a repetition rate of typically 50 kHz. Two different kinds of spectra can be recorded. For Zeeman spectra the laser wavelength is fixed and the external B field is swept typically up to 50 μT, while for optical spectra the Zeeman field is fixed and the wavelength is scanned. The data were recorded by a personal computer and subsequently processed on a Hewlett-Packard HP1000 computer.

For the conditions met in this experiment the Doppler linewidth [full width at half maximum (FWHM)] is approximately 600 MHz and the pressure broadening is of the same order of magnitude. The hyperfine splittings of ^{85}Rb and ^{87}Rb are 6.84 and 3.04 GHz, respectively, for the ground state (and 0.82 and 0.36 GHz, respectively, for the excited state). Therefore the homogeneously broadened four-level model system in Sec. II can only be a rough approximation of the complicated level scheme of rubidium. To a first approximation the total number of four hyperfine split optical transitions for each Rb isotope can be regarded as a superposition of eight optical transitions. For external B fields considered here the Zeeman level spacings within a hyperfine level were equivalent, i.e., well within the linear regime of the Breit-Rabi formula,[19] and only a single value for the ground-state splitting is expected for each isotope, which is given by the gyromagnetic ratios of $\gamma_{85}=2\pi\times 4.6708$ kHz/μT and $\gamma_{87}=2\pi\times 7.006$ kHz/μT for ^{85}Rb and ^{87}Rb, respectively.

IV. RESULTS AND DISCUSSION

As described in the previous sections, in order to produce a considerable amount of spin polarization in the ground state it is essential to be close to optical resonance with the pump laser wavelength and also have an integer multiple of the pump pulse repetition rate match the ground-state splitting of interest.

Figure 5 shows the initial buildup of spin polarization in the Zeeman sublevels of the $F=3$ hyperfine level of ^{85}Rb in its $5\,^2S_{1/2}$ ground state after the periodic pump pulse sequence is turned on at $t=0$. At $t<0$ the spin ensemble is in thermal equilibrium, where no magnetization in the propagation direction of the pump or probe beams (z direction) is present and therefore no MCD or MOR signals are detectable that are due to the sample. Static magneto-optical effects from the glass container and optical components are nulled by orienting the polarimeter properly. The upper trace in Fig. 5 shows the pump pulses of duration $t_p=6.4$ μs at a repetition rate of $\nu_{\rm rep}=50$ kHz. When the external field is tuned to a value where the Larmor frequency $\Omega_L=\gamma_{85}B=2\pi\times 50$ kHz an oscillating MCD signal is detected, which is shown in the lower trace. The two traces have the same periodicity since we adjusted the first-order Zeeman resonance [$k=1$ in Eq. (2.3)]. A similar signal is observed when tuning the laser to the ^{87}Rb optical resonance and adjusting the magnetic field according to $\gamma_{87}B=2\pi\times 50$ kHz. In both cases the precessing magnetization is resonantly enhanced until it reaches a quasistationary value after several pulses. The time constant and the stationary peak value depend on the pump pulse power and the relaxation rate Γ between Zeeman levels. In our case Γ is given by the rate the atoms escape from the laser beam region and is on the order of 10^4 s^{-1}. Note that Γ ultimately limits the number of pulses after which the stationary state is reached. It is also seen from Fig. 5(b) that not only the oscillating magnetization increases, but in addition a dc offset builds up. This phenonemon has been described in

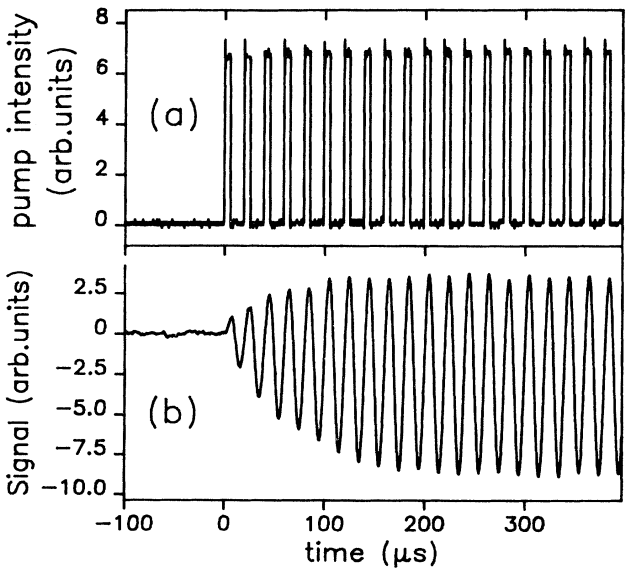

FIG. 5. (a) Pump pulse intensity for periodic excitation of spin coherence starting at $t=0$ ($\nu_{\rm rep}=50$ kHz, $t_p=6.4$ μs, optical wavelength corresponds to the $F=3\rightarrow F'=2$ transition of ^{85}Rb). (b) MCD-detected buildup of precessing magnetization. The external B field is set for the Larmor frequency of ^{85}Rb to match the repetition rate of the optical pulses ($B=10.70$ μT).

detail in Ref. 20, where the response of the system to a step input cw pump beam is considered and after a time of several $1/\Gamma_{\text{eff}}$ a static magnetization is found. In our case a considerable time after the initial transient response to the periodic pulse sequence has reached its stationary state, spectra are taken by recording the peak MCD or MOR signal as a function of the laser wavelength and as a function of the B field, which controls the Zeeman level splittings.

In Fig. 6 two Zeeman spectra are displayed, where the B field is scanned while the laser wavelength is kept constant. In Fig. 6, curve (a), the laser is tuned to the $F=3\rightarrow F'=2$ transition of the ^{85}Rb D_1 line, so only the corresponding ground-state Zeeman transition of ^{85}Rb is measured. Measurement of the Zeeman splitting of the other isotope is discriminated against: The laser is too far off the ^{87}Rb optical resonance for optically pumping spin polarization for this isotope, which is a prerequisite for detecting the signal. In Fig. 6, curve (b), the situation is reversed. We tuned the laser to an optical resonance of ^{87}Rb ($F=2\rightarrow F'=1$) and consequently the ^{85}Rb Zeeman resonance is suppressed. Having the laser tuned to a particular optical transition of one isotope, only the ground state belonging to this transition may gain polarization due to the periodic excitation scheme, if in addition to the optical resonance also the Zeeman resonance is adjusted according to Eq. (2.3). The ground-state splitting of the species not in optical resonance with the laser is not detected, although it falls within the field range covered. The suppression of the Zeeman transition within the unpumped ground state is not perfect because of small off-resonance pumping effects and the limited frequency stability of the laser used. Also polarization transferred from the pumped species to the unpumped by collisions would be noticeable in a nonperfect suppression of the unpumped isotope line. Measuring the unpumped Zeeman line intensity may even be used to study spin-exchange kinetics and mechanisms among different isotopes. Since the gyromagnetic ratios γ_{85} and γ_{87} of ground-state ^{85}Rb and ^{87}Rb are known to very high precision, the separation of these lines can be utilized to measure the B field very accurately. In fact, we used it to calibrate our B field setup.

Zeeman spectra of the type shown in Fig. 6 were recorded for optical wavelengths spanning the entire spectral region of the Rb D_1 line. They are depicted in Fig. 7 in a perspective fashion. Here second-order Zeeman resonance ($k=2$) is recorded as compared to first order ($k=1$) in Fig. 6. This shifts the resonance B field up by a factor of 2, whereas the spectral features remain unchanged. Note the huge difference in the frequency scales of the two axes. The optical axis spans 10 GHz whereas the B field corresponds to roughly 100 kHz, more than three orders of magnitude below the Doppler linewidth. Along the B axis there are two groups of lines corresponding to the ground-state Zeeman splittings of

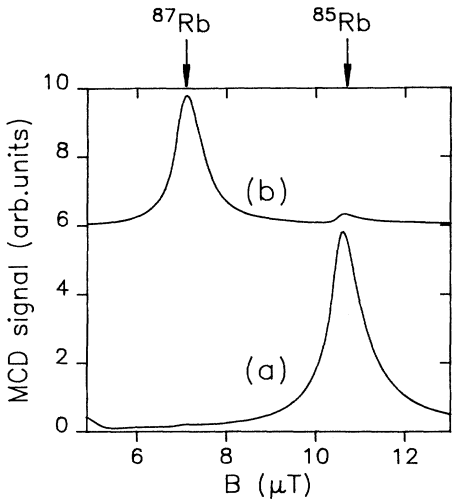

FIG. 6. First-order ($k=1$) ground-state Zeeman spectrum of atomic Rb as detected by the MCD of the periodically pumped gas. When the optical wavelength is set to the $F=3\rightarrow F'=2$ transition of ^{85}Rb [curve (a)] only the ^{85}Rb Zeeman transition is detected and ^{87}Rb is suppressed, whereas only the ^{87}Rb transition is detected [curve (b)] if the laser is tuned to a ^{87}Rb optical transition, $F=2\rightarrow F'=1$ in this case. The expected Zeeman transitions are indicated by the arrows ($\nu_{\text{rep}}=50$ kHz, $t_p=1$ μs).

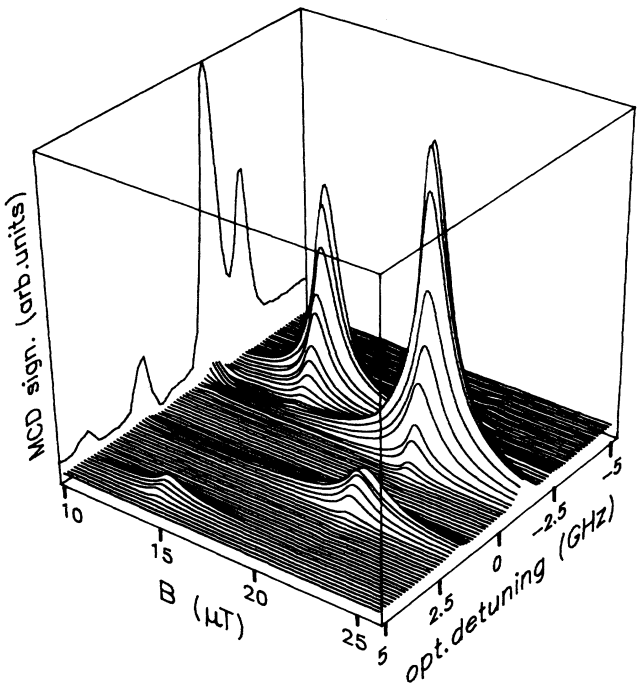

FIG. 7. MCD signal detected as a function of the external B field and as a function of the laser wavelength for $\nu_{\text{rep}}=50$ kHz. The entire 2D data field is recorded by scanning the B field for constant optical frequencies separated by roughly 125 MHz. The optical frequency is referenced to the D_1 line center of ^{85}Rb, i.e., 794.76 nm. The B field covers the range of second-order Zeeman resonance ($k=2$) for both isotopes. The projection onto the optical axis is also shown, representing the optical absorption spectrum of the isotopically mixed Rb sample. Along the B field axis the superimposed spectra of the two isotopes are separated due to their different ground-state gyromagnetic ratios.

the two isotopes as already shown in Fig. 6. The origin of the optical frequency axis is set to the ^{85}Rb D_1 line center at $\lambda = 794.76$ nm and positive detunings mean higher energy quanta. Along this axis four hyperfine (hf) split optical transitions are expected for each isotope. Two of these are clearly resolved, the observed splitting corresponding to the ground-state hf splitting of 6.84 and 3.04 GHz for ^{87}Rb and ^{85}Rb, respectively. The excited-state hf splittings of 0.82 GHz (^{87}Rb) and 0.36 GHz (^{85}Rb) are not readily resolved in the MCD detection mode. Also shown in Fig. 7 is the projection of the 2D spectrum onto the optical axis. Except for line intensities this has to be identified with the optical absorption spectrum of Rb vapor taken, for example, with a regular absorption spectrometer. It shows eight spectral lines in a narrow region, four of which are resolved here. Without further information the individual lines can not be attributed to the different isotopes. But recording the full 2D spectrum the superimposed optical spectra of the isotope mixture can be disentangled and are separated along the second axis introduced, which distinguishes between different ground-state Zeeman splittings. Optical transitions belonging to the same ground-state splitting appear on a line parallel to the optical frequency axis and thus are assigned to one isotope in this case.

In order to get higher optical resolution, the dispersive MOR detection mode is used. A complete 2D spectrum is shown in Fig. 8, where the MOR signal is recorded instead of the MCD signal in Fig. 7. The contour plot shows the lines connecting points of equal signal altitude, where solid (dashed) lines correspond to positive (negative) MOR signals. The improved resolution of MOR versus MCD detection is most clearly demonstrated by the spectral feature in the lower left corner of Fig. 8, which can only be explained by a superposition of two dispersive lines close to each other. The asymmetry of the dispersion line in the upper part of the spectrum also gives a hint that there are two lines at different frequencies superimposed on each other.

In order to get separated optical spectra of the species involved, vertical cross sections are taken at the resonating B fields of the isotopes of interest. Two of these cross sections are shown in Fig. 9 for the Zeeman resonance fields of ^{85}Rb and ^{87}Rb, respectively. The anticipated hf split optical transitions are indicated by stick diagrams. Note that the optical spectra are completely separated showing no features of the other isotope, although both species are present in the sample at the same time and are exposed to the same light. For both isotopes the ground-state hf splitting is resolved, whereas the excited-state hf splitting is only resolved for ^{87}Rb. Resolving the corresponding excited-state hf splitting of ^{85}Rb is obscured by the pressure broadened homogeneous linewidth and laser frequency jitter but the asymmetry in the dispersive lines is an indication for having more than one line present.

The line intensities observed depend on the particular optical pumping pathway of this multilevel system and are not further investigated here. They reflect the extent to which optical pumping is efficient for the individual hf split optical transitions under otherwise identical conditions. Transitions having the largest optical spin pumping rates appear as the most intense lines in these spectra. Pumping different hf split optical transitions may even lead to different signs of the ground-state polarization created, as is demonstrated by the W-shaped structure in the left part of the ^{87}Rb spectrum in Fig. 9.

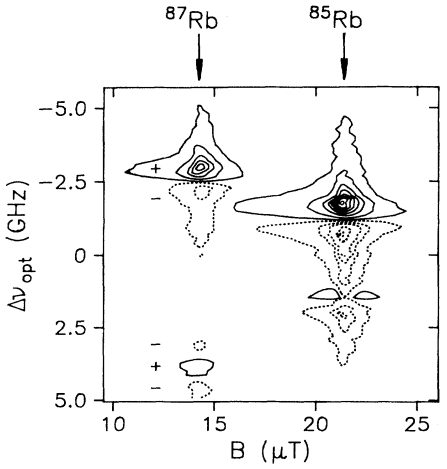

FIG. 8. Contour plot of the MOR-detected signal, which shows dispersive line shapes along the optical axis. Full (dashed) lines represent positive (negative) signals. Arrows indicate second-order ($k = 2$) Zeeman resonance of the two isotopes (all other parameters same as Fig. 7).

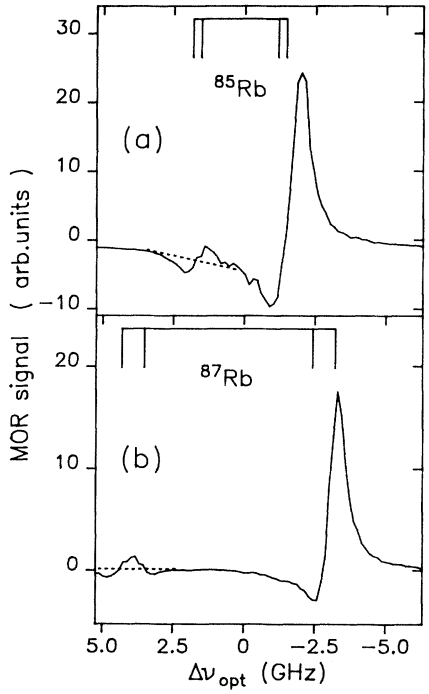

FIG. 9. Vertical cross sections through the 2D MOR-detected signal data set of Fig. 8 at B field values, where ^{85}Rb (a) and ^{87}Rb (b) have their ground-state Zeeman resonances, respectively, showing the clear separation of spectra of the two isotopes in the isotopically mixed sample. The expected hyperfine split optical transitions are indicated.

V. CONCLUSIONS

Zeeman selective optical spectroscopy, which allows for spectral separation of different isotopes, has been demonstrated in a two-dimensional optical fashion. The two relevant frequency axes are the Zeeman frequency Ω_L and the optical transition frequencies of the different isotopes. Resonance along the Zeeman axis occurs, if the light field is amplitude modulated at the ground-state splitting frequency, while optical resonance occurs, if the optical carrier frequency coincides with an optical transition frequency. A 2D resonance peak appears, whenever both optical and Zeeman resonance conditions are met simultaneously, giving rise to the separation of optical spectra grouped according to their ground-state sublevel splitting. The method is applicable in all cases where the light pulse repetition rate (or multiples thereof) can be made comparable to the sublevel splitting and pulse durations are short compared to the inverse of the splitting frequency. The individual 2D line shapes can be calculated from a simple Bloch-type equation, when excited-state effects are negligible. The potential of the method is twofold, (i) the amplitudes of the sublevel coherences are increased far over the single pulse excitation amplitudes due to the repetitive in-phase excitation, and (ii) other modes with different frequencies are discriminated against due to the selectivity of the method. In addition, the selectivity with respect to optical transitions of the sample is used.

ACKNOWLEDGMENTS

We would like to acknowledge discussions with J. Mlynek and D. Suter and appreciate receiving papers from them prior to publication. We thank A. Sailer for his help in the early stage of the experiments and H. Nebenführ for making available his comfortable 2D data handling programs. The Deutsche Forschungsgemeinschaft has given financial support under SFB 228.

APPENDIX: FOURIER ANALYSIS OF PERIODIC EXCITATION

Starting from an alternative notation of Eq. (2.1), namely,

$$\dot{\mathbf{m}}(t)=\tilde{A}\mathbf{m}(t)+\mathbf{P}(t)\ , \tag{A1}$$

where the pulsed light excitation is expressed as

$$\mathbf{P}(t)=\begin{cases}(0,0,P_+) & \text{for } nT-t_p/2\le t<t_p/2+nT,\\ (0,0,0) & \text{for } nT-T/2\le t<nT-t_p/2\ ,\\ (0,0,0) & \text{for } nT+t_p/2\le t<nT+T/2,\end{cases} \tag{A2}$$

and where

$$\tilde{A}=\begin{pmatrix}-\Gamma_{\text{eff}} & -\Omega_z & 0\\ \Omega_z & -\Gamma_{\text{eff}} & -\Omega_x\\ 0 & \Omega_x & -\Gamma_{\text{eff}}\end{pmatrix}\ , \tag{A3}$$

with $\Gamma_{\text{eff}}=\Gamma+P_+(t_p/T)$ and $\Omega_z=P_+\bar{\Delta}(t_p/T)$. Note that $\tilde{A}$ is made independent of time by inserting average values for Γ_{eff} and Ω_z. This approximation is justified, if one deals with small pumping rates P_+, as realized in our experiments. Once the initial transients have decayed, a steady state is reached, which may be expressed by the Fourier series:

$$\mathbf{m}(t)=\frac{\mathbf{a}_0}{2}+\sum_{k=1}^{\infty}[\mathbf{a}_k\cos(k\omega_0 t)+\mathbf{b}_k\sin(k\omega_0 t)]\ , \tag{A4}$$

with the usual definition for a_k and b_k, and $\omega_0=2\pi\nu_{\text{rep}}=2\pi/T$ is the fundamental frequency, given by the period of the excitation cycle. In the lock-in detection scheme used here the coefficients a_k and b_k are measured directly, k depending on the reference frequency $k\omega_0$ employed. The pulsed light sequence leads to

$$P_+(t)=P_+\left[\frac{t_p}{T}\right]+\sum_{k=1}^{\infty}[p_k\cos(k\omega_0 t)]\ , \tag{A5}$$

with

$$p_k=2P_+\left[\frac{t_p}{T}\right]\frac{\sin\left[\frac{k\omega_0 t_p}{2}\right]}{\left[\frac{k\omega_0 t_p}{2}\right]}\ . \tag{A6}$$

After some algebra we arrive at

$$\mathbf{a}_0=-2\frac{t_p}{T}\tilde{A}^{-1}\mathbf{P}\ , \tag{A7}$$

$$\mathbf{a}_k=-\left[\tilde{1}+\frac{\tilde{A}^2}{(k\omega_0)^2}\right]^{-1}\frac{\tilde{A}}{k\omega_0}\cdot\frac{\mathbf{p}_k}{k\omega_0}\ , \tag{A8}$$

$$\mathbf{b}_k=-(k\omega_0)\tilde{A}^{-1}\mathbf{a}_k\ , \tag{A9}$$

where $\mathbf{p}_k=(0,0,p_k)$ and $\mathbf{P}=(0,0,P_+)$. The optical detection scheme applied here allows the detection of the magnetization component $m_z(t)$ perpendicular to the magnetic field B. Therefore we restrict ourselves to the calculation of the z component only. The base-line offset $a_{0z}/2$ is readily obtained from Eq. (A7) as

$$a_{0z}=P_+\left[\frac{t_p}{T}\right]\frac{\Gamma_{\text{eff}}^2+\Omega_z^2}{\Gamma_{\text{eff}}(\Gamma_{\text{eff}}^2+\Omega_x^2+\Omega_z^2)}\ . \tag{A10}$$

The "absorptive" part at frequency $k\omega_0$ is obtained from Eq. (A8) as

$$a_{kz}=\Gamma'\left[\frac{p_k}{k\omega_0}\right]\frac{R(\Omega_L,\bar{\Delta})}{Q(\Omega_L,\bar{\Delta})}\ , \tag{A11}$$

with p_k given by Eq. (A6), where

$$R(\Omega_L,\bar{\Delta})=(1-\Gamma'^2)^2+\Omega_x'^2(1+\Gamma'^2+\Omega_z^2)-2\Omega_z'^2(1-\Gamma'^2)+\Omega_z'^4 \tag{A12}$$

and

$$Q(\Omega_L,\bar{\Delta})=(1+\Gamma'^2)[(1+\Gamma'^2)^2+(\Omega_x'^4+\Omega_z'^4)-2\Omega_x'^2(1-\Gamma'^2-\Omega_z'^2)-2\Omega_z'^2(1-\Gamma'^2)]\ , \tag{A13}$$

where the prime denotes normalization to the reference frequency used:

$$\Omega'_x=\frac{\Omega_L}{k\omega_0},\quad \Omega'_z=\frac{P_0}{k\omega_0}\frac{\bar{\Delta}}{1+\bar{\Delta}^2},\quad \Gamma'=\frac{\Gamma_{\text{eff}}}{k\omega_0}\ . \tag{A14}$$

The z component of the full two-dimensional magnetization response is represented by a_{kz}, according to Eq. (A11). Let us discuss the two most interesting limiting cases, where at least one of the two resonance conditions is fulfilled.

(i) For the optical on-resonance case ($\bar{\Delta}=0$, $\Omega'_z=0$) we obtain

$$a_{kz}(\Omega_L)\propto\frac{R(\Omega_L,0)}{Q(\Omega_L,0)}=\frac{1+\Gamma'^2+\Omega'^2_x}{(1+\Gamma'^2)^2+\Omega'^2_x[\Omega'^2_x-2(1-\Gamma'^2)]}\ . \tag{A15}$$

This represents a Zeeman resonance line for $\Omega'_x\approx 1$, i.e., $\Omega_L\approx k\omega_0$, with a half width, which is a function of $\Gamma'=\Gamma_{\text{eff}}/(k\omega_0)$.

(ii) For the Zeeman on-resonance case ($\Omega'_x=1$, $\Omega_L=k\omega_0$) we get

$$a_{kz}(\bar{\Delta})\propto\Gamma'\left[\frac{P_0}{1+\bar{\Delta}^2}\right]\frac{R(1,\bar{\Delta})}{Q(1,\bar{\Delta})}=\Gamma'\left[\frac{P_0}{1+\bar{\Delta}^2}\right]\frac{(1+\Gamma'^2)(2+\Gamma'^2)-\Omega_z'^2(1-2\Gamma'^2-\Omega'^2_z)}{(1+\Gamma'^2)[\Gamma'^2(4+\Gamma'^2)+\Omega'^2_z(2\Gamma'^2+\Omega'^2_z)]}\ . \tag{A16}$$

This expression yields the optical resonance line near $\bar{\Delta}\approx 0$. The full plot of Eq. (A11) as a function of Ω_L and $\bar{\Delta}$ gives qualitatively the same result as already given in Fig. 3 of Sec. II.

[1]W. Happer, Rev. Mod. Phys. **44**, 169 (1972); C. Cohen-Tannoudji, in *Atomic Physics,* edited by G. zu Putlitz, E. W. Weber, and A. Winnacker (Plenum, New York, 1975), Vol. 4.

[2]H. G. Dehmelt, Phys. Rev. **105**, 1924 (1957).

[3]N. Bloembergen, P. Pershan, and L. Wilcox, Phys. Rev. **120**, 2014 (1960).

[4]W. E. Bell and A. L. Bloom, Phys. Rev. **107**, 1559 (1957).

[5]J. Dodd, W. Fox, G. W. Series, and M. Taylor, Proc. Phys. Soc. (London) **74**, 789 (1959).

[6]Y. Fukuda, J. Hayashi, K. Kondo, and T. Hashi, Opt. Commun. **38**, 357 (1981).

[7]H. Harde and H. Burggraf, Opt. Commun. **40**, 441 (1982); J. Mylnek, W. Lange, H. Harde, and H. Burggraf, Phys. Rev. A **24**, 1099 (1981).

[8]H. Lehmitz, W. Kattau, and H. Harde, in *Methods of Laser Spectroscopy,* edited by Y. Prior, A. Ben-Reuven, and M. Rosenbluh (Plenum, New York, 1986), p. 97.

[9]Y. Fukuda, Y. Takagi, and T. Hashi, Phys. Lett. **48A**, 183 (1974).

[10]A. M. Wiener, D. E. Leaird, G. P. Wiederrecht, and K. A.Nelson, Science **247**, 1317 (1990).

[11]G. A. Morris and R. Freeman, J. Magn. Res. **29**, 433 (1978).

[12]F. Mitschke, R. Deserno, W. Lange, and J. Mlynek, Phys. Rev. A **33**, 3219 (1986).

[13]M. Kitano, T. Yabuzaki, and T. Ogawa, Phys. Rev. A **24**, 3156 (1981).

[14]R. P. Feynman, F. L. Vernon, and R. W. Hellwarth, J. Appl. Phys. **28**, 49 (1957).

[15]R. R. Ernst, G. Bodenhausen, and A. Wokaun, *Principles of Nuclear Magnetic Resonance in One and Two Dimensions* (Clarendon, Oxford, 1987), Chap. 6.

[16]P. Scheufler, K. D. Dünnebeil, Th. Vetter, and M. Mehring, in *High Precision Navigation,* edited by K. Linkwitz and U. Hangleiter (Springer, Berlin, 1989), p. 602.

[17]R. V. Jones, Proc. R. Soc. London, Ser. A **349**, 423 (1976).

[18]T. Kohmoto, Y. Fukuda, and T. Hashi, Phys. Rev. B **34**, 6085 (1986).

[19]G. Breit and I. I. Rabi, Phys. Rev. **38**, 2082 (1931).

[20]D. Suter, M. Rosatzin, and J. Mylnek, Phys. Rev. A **41**, 1634 (1990).